Deep Inference for Covariance Estimation: Learning Gaussian Noise Models for State Estimation

Deep Inference for Covariance Estimation: Learning Gaussian Noise Models for State Estimation

Katherine Liu*, Kyel Ok*, William Vega-Brown, and Nicholas Roy

***Abstract*— We present a novel method of measurement covariance estimation that models measurement uncertainty as a function of the measurement itself. Existing work in predictive sensor modeling outperforms conventional fixed models, but requires domain knowledge of the sensors that heavily influences the accuracy and the computational cost of the models. In this work, we introduce Deep Inference for Covariance Estimation (DICE), which utilizes a deep neural network to predict the covariance of a sensor measurement from raw sensor data. We show that given pairs of raw sensor measurement and ground-truth measurement error, we can learn a representation of the measurement model via supervised regression on the prediction performance of the model, eliminating the need for hand-coded features and parametric forms. Our approach is sensor-agnostic, and we demonstrate improved covariance prediction on both simulated and real data.**

I. Introduction

We are interested in developing better models of sensor uncertainty to improve the state estimation performance of unmanned vehicles. Sensor noise characteristics are fundamental to applications such as the optimal fusion of measurements from several noisy sensors into a single estimate of the vehicle state. Even on vehicles with a single sensor, noise characteristics are key to evaluating the uncertainty in past estimates and reducing the accumulated error in the presence of additional sources of information, e.g., loop-closure detections added to visual odometry.

Sensor measurements are commonly modeled as Gaussian random variables, conditioned upon the state from which the measurement was taken. The covariance of these random variables is often assumed to be a constant term either set by hand or derived from empirical data. However, this approach to noise specification is prone to error due to the sensor performance being a function of the environment and the assumptions of the measurement process. For example, a visual odometry measurement relies on camera images and a process (such as [1], [2]) that aligns the images of a static, textured, and constantly-bright environment. Consequently, the accuracy of the measurements in dynamic scenes such as the one in Fig. 1, low texture environments, and poor lighting conditions is often degraded.

Previous work in modeling sensor noise as a function of the environment required significant domain knowledge and could not easily generalize to an arbitrary high-dimensional sensor. Vega-Brown et al. proposed a non-parametric kernel estimation technique for covariance estimation, CELLO [3], which approximated sensor noise as the empirical covariance of neighboring training data in a hand-coded feature space. While this approach is effective for simple sensors, it is challenging to hand-specify predictive features for complex sensors such as a camera-based visual odometry sensor. Furthermore, the approach required online kernel regression on the training data, which scales poorly with the size of the data and the complexity of the problem. Similarly, [4] relied on hand-coded features, but addressed the scalability problem by learning a parametric function of the features offline. However, this approach required even more domain knowledge, as both the parametric form of the sensor noise and the predictive features must be specified.

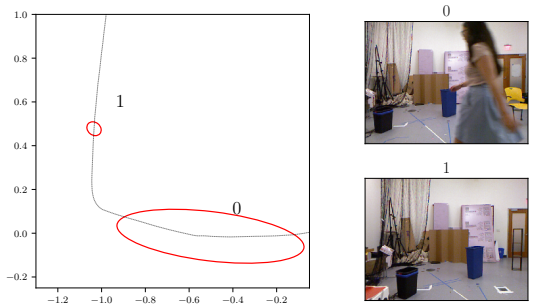

Fig. 1: Example measurement covariances (red) shown for static and dynamic scenes. The visual odometry is corrupted by a person walking through the scene (frame 0). DICE correctly predicts an elongated covariance in the direction of the person's motion, where noise was added, and reduces the covariance after the person has exited the scene (i.e., frame 1). The covariance is scaled here for visualization.

We introduce Deep Inference for Covariance Estimation (DICE), a constant time method for predicting the measurement uncertainty of a highly complex sensor that does not require any domain knowledge. We train a deep convolutional neural network to learn the noise model of a sensor measurement as a function of the pre-processed raw measurement, while also constraining the covariance predictions to be well-formed, i.e., positive definite. This novel approach does not rely on specifying an exact parametric form for the noise model or the predictive features in the model, and scales well with the complexity of the problem, due to an offline utilization of the training data.

In the following sections, we describe our approach and show that we can learn the measurement uncertainty of highly complex sensors, thereby improving the performance of state estimation.

*The first two authors contributed equally to this paper.

All authors are with the Computer Science and Artificial Intelligence Laboratory (CSAIL), Massachusetts Institute of Technology, Cambridge, MA 02139, USA {katliu,kyelok,wrvb,nickroy}@mit.edu

II. PRELIMINARIES

We consider a robot with state $\boldsymbol{x}_i \in \mathbb{R}^n$, equipped with a sensor providing a direct measurement $\boldsymbol{z}_i \in \mathbb{R}^p$, where $p \leq n$, at each time step i. We assume that the measurement process may consist of an initial stage to obtain a high dimensional raw measurement $\boldsymbol{\xi}_i \in \mathbb{R}^m$ and a follow-up stage to process the raw measurement into a direct measurement $\boldsymbol{z}_i$ of the state. For example, a GPS sensor first obtains a raw measurement $\boldsymbol{\xi}_i$ of time-of-flight to satellites, then processes it via multilateration to obtain a direct measurement $\boldsymbol{z}_i$ of the sensor position $\boldsymbol{x}_i$, i.e., $\boldsymbol{z}_i = alg(\boldsymbol{\xi}_i)$ where $p = n$. We call $\boldsymbol{z}_i$ a *direct* measurement for observing all or a part of the state, as opposed to $\boldsymbol{\xi}_i$, which is a high dimensional measurement of the world such as images, laser scans, etc.

We assume Gaussian distributions for the conditional probabilities of observation $p(\boldsymbol{z}_i|\boldsymbol{x}_i)$ and state transition $p(\boldsymbol{x}_i|\boldsymbol{x}_{i-1})$. Given appropriate functions for expected state transition $f(\boldsymbol{x})$ and observation $h(\boldsymbol{x})$ along with their uncertainties in the form of positive definite covariance matrices $\boldsymbol{Q}_i \in \mathbb{R}^{n\times n}$ and $\boldsymbol{R}_i \in \mathbb{R}^{p\times p}$, we can write

$$\begin{aligned} \boldsymbol{x}_i &\sim \mathcal{N}(f(\boldsymbol{x}_{i-1}), \boldsymbol{Q}_i) \\ \boldsymbol{z}_i &\sim \mathcal{N}(h(\boldsymbol{x}_i), \boldsymbol{R}_i). \end{aligned} \tag{1}$$

The measurement model h for processed direct measurements can typically be written in the form $h(\boldsymbol{x}_i) = \boldsymbol{P}\boldsymbol{x}_i$, where $\boldsymbol{P} \in \mathbb{R}^{p\times n}$.

Most probabilistic state estimation methods utilize the covariance terms $\boldsymbol{Q}_i$ and $\boldsymbol{R}_i$ to determine the optimal weighting of the different sources of information. For example, optimizing the trajectory of a robot equipped with a single sensor can be written as a least-squares problem [5]

$$\underset{\boldsymbol{x}_{0:N}}{\arg\min} \Big\{ \sum_i^N \|f(\boldsymbol{x}_{i-1}) - \boldsymbol{x}_i\|^2_{\boldsymbol{Q}_i} + \sum_i^N \|h(\boldsymbol{x}_i) - \boldsymbol{z}_i\|^2_{\boldsymbol{R}_i} \Big\}, \tag{2}$$

where $\|\boldsymbol{e}\|^2_\Sigma$ is the Mahalanobis norm that directly scales the modeling error $\boldsymbol{e}$ inversely proportional to the square root of the covariance term Σ, i.e., $\|\boldsymbol{e}\|^2_\Sigma \triangleq \boldsymbol{e}^\mathsf{T}\Sigma^{-1}\boldsymbol{e} = \|\Sigma^{-\mathsf{T}/2}\boldsymbol{e}\|^2_2$.

As such, the optimal values of the estimated states are sensitive to the measurement covariances, and we aim to better estimate the measurement covariances in order to improve the overall performance of state estimation.

III. APPROACH

A. Problem Formulation

We would like to predict the distribution over sensor measurement error $\boldsymbol{e}_i \in \mathbb{R}^p$, conditioned on the raw measurement $\boldsymbol{\xi}_i$, i.e., predict the distribution $p(\boldsymbol{e}_i|\boldsymbol{\xi}_i)$. Assuming the distribution to be a zero-mean Gaussian (assuming an un-biased sensor), we focus on predicting the covariance $\boldsymbol{R}_i$ of the distribution as a function of the raw measurement $\boldsymbol{\xi}_i$, i.e., forming the predictive function g where

$$\boldsymbol{R}_i \approx g(\boldsymbol{\xi}_i). \tag{3}$$

The approximator function g must capture the highly complex mapping between the raw sensor data to the covariance matrix $\boldsymbol{R}_i$. One way to predict a complex mapping is by over-parameterizing the approximator function, then learning the parameters using a labeled training dataset $\mathcal{D}$. If an ideal training dataset $\mathcal{D} = \{\boldsymbol{\xi}_i, \mathcal{N}(0, \boldsymbol{R}_i) | \forall i \in [1, V]\}$ is available (where $\boldsymbol{\xi}_i$ is a raw measurement and $\mathcal{N}(0, \boldsymbol{R}_i)$ the distribution over measurement error), one could directly minimize the distance between the predicted distribution $\mathcal{N}(0, g(\boldsymbol{\xi}_i))$ and the true distribution $\mathcal{N}(0, \boldsymbol{R}_i)$ by using a distance metric between distributions.

However, there are two complications to this approach. First, it is often difficult to obtain the true distribution over measurement error $\mathcal{N}(0, \boldsymbol{R}_i)$ during training time. Second, the approximator function g must only produce positive definite covariance matrices, i.e., the optimization is constrained subject to $v^\mathsf{T}\boldsymbol{R}_i v > 0$ for any non-zero $v \in \mathbb{R}^n$.

To overcome these difficulties, we instead maximize the likelihood of drawing each measurement error $\boldsymbol{e}_i$ from a predicted distribution $\mathcal{N}(0, g(\boldsymbol{\xi}_i))$, foregoing the need for the true distribution, and add a decomposition to the approximator function g to relax the constraint for positive definiteness in the optimization. In the following sections, we describe the details of the function approximator and discuss the changes needed to robustly predict measurement covariances without requiring difficult-to-obtain training data.

B. Deep Convolutional Neural Network

In order to learn the complex mapping g between the raw measurement $\boldsymbol{\xi}_i$ and the covariance matrix $\boldsymbol{R}_i$, we utilize an over-parametrized form of the approximator function. We take a similar approach to that of recent successes [6], [7] and choose a deep convolutional neural network (CNN), shown in Fig. 2, as our parameterization.

Let $f_k(\boldsymbol{\xi}_i; \boldsymbol{K}_1, ..., \boldsymbol{K}_k, \boldsymbol{B}_1, ..., \boldsymbol{B}_k) \mapsto \mathbb{R}^r$ be a convolutional neural network with k convolutional filters, where the parameters being optimized are convolutional filters $\boldsymbol{K}_{1:k} \in \mathbb{R}^{q\times s\times t}$ and bias matrices $\boldsymbol{B}_{1:k} \in \mathbb{R}^{u\times v}$. Cascaded operations of strided multi-channel convolution and non-linear activation function (with optional max-pooling) reduce the high-dimensional raw measurement $\boldsymbol{\xi}_i \in \mathbb{R}^m$ down to a set of low-dimensional features, which are then vectorized such that $f_k(\boldsymbol{\xi}_i) \in \mathbb{R}^r$, i.e., $r \ll m$. These feature responses are analogous to the hand-coded features in [4], and as done in previous work, we linearly combine them to produce a vectorized form of the covariance matrix:

$$\boldsymbol{r}_i \approx g(\boldsymbol{\xi}_i) = \boldsymbol{W} \cdot f_k(\boldsymbol{\xi}_i) + \boldsymbol{b}. \tag{4}$$

Our method combines the optimization of feature representation, i.e., the convolutional filters $\boldsymbol{K}_{1:k}$ and the bias matrices $\boldsymbol{B}_{1:k}$, as well as the weighting, i.e., the weight matrix $\boldsymbol{W} \in \mathbb{R}^{n\times r}$ and the bias vector $\boldsymbol{b} \in \mathbb{R}^n$, of the features $f_k(\boldsymbol{\xi}_i) \in \mathbb{R}^r$ to predict the final covariance parameters $\boldsymbol{r}_i \in \mathbb{R}^{n\times n}$. The optimized features are therefore tailored for accurate covariance prediction and do not require hand-coding. Additionally, after the network parameters have been optimized, covariance prediction is simply the evaluation of the raw sensor data through the network, and is therefore constant time, and real-time for moderate network sizes.

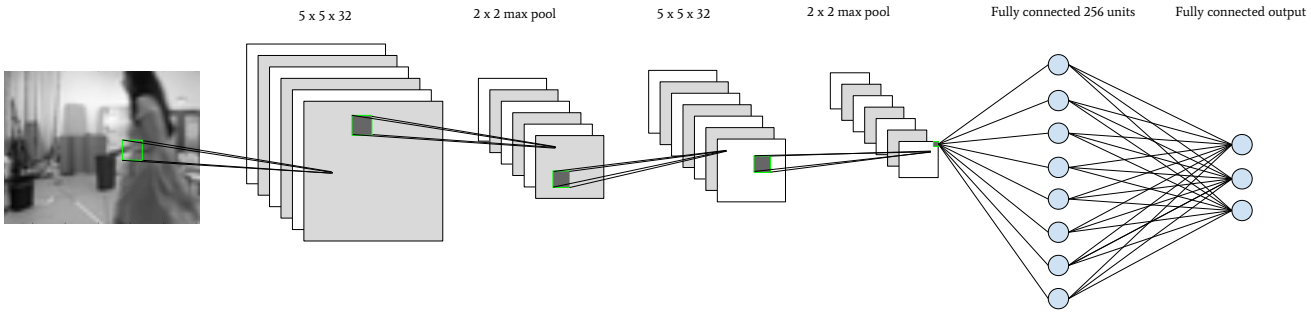

Fig. 2: Neural network architecture used to approximate the covariance prediction function. The input to the network is the raw measurement, e.g., a (possibly) down-scaled camera image, and the output is the vector of the free parameters of the covariance. The narrowing architecture in the beginning reduces the raw measurement into low-dimensional features, and the following fully-connected layer optimally combines the features for the covariance prediction task.

C. Likelihood Loss Function

Given a training dataset $\mathcal{D} = \{\boldsymbol{\xi}_i, \mathcal{N}(0, \boldsymbol{R}_i) | \forall i \in [1, V]\}$ of pairs of raw measurement $\boldsymbol{\xi}_i$ and a distribution over measurement error $\mathcal{N}(0, \boldsymbol{R}_i)$, one could optimize for the parameters $G = \{\boldsymbol{K}_j, \boldsymbol{B}_j, \boldsymbol{W}, \boldsymbol{b} | \forall j \in [1, k]\}$ of the neural network by directly minimizing a distance metric such as Kullback-Leibler divergence between the predicted and the true distributions, i.e.,

$$\arg\min_{G} \sum_{i=1}^{V} \mathrm{KL}(\mathcal{N}(0, g(\boldsymbol{\xi}_i)) || \mathcal{N}(0, \boldsymbol{R}_i)). \tag{5}$$

However, it is infeasible to obtain the true distribution over sensor measurement errors. Instead, it is much easier to obtain measurement errors $\boldsymbol{e}_i$ (drawn from $\mathcal{N}(0, \boldsymbol{R}_i)$), given a reliable sensor such as an indoor positioning system (IPS) that can obtain the same measurement $\boldsymbol{z}_i^*$ with higher precision and accuracy. Therefore, one can more conveniently obtain a training dataset $\mathcal{D} = \{\boldsymbol{\xi}_i, \boldsymbol{e}_i | \forall i \in [1, V]\}$ where $\boldsymbol{e}_i$ is the error made by the sensor, i.e., $\boldsymbol{e}_i = \left| \boldsymbol{z}_i^* - \boldsymbol{z}_i \right|$.

Given the training dataset $\mathcal{D} = \{\boldsymbol{\xi}_i, \boldsymbol{e}_i\}$ of raw measurements $\boldsymbol{\xi}_i$ and measurement errors $\boldsymbol{e}_i$, we can instead maximize the likelihood of drawing the measurement errors from the distribution over the errors

$$\arg\max_{\boldsymbol{R}_{1:V}} \sum_{i=1}^{V} p\left(\boldsymbol{e}_i | \boldsymbol{R}_i\right), \tag{6}$$

or minimize the negative log-likelihood

$$\arg\min_{\boldsymbol{R}_{1:V}} \sum_{i=1}^{V} -\log(p\left(\boldsymbol{e}_i | \boldsymbol{R}_i\right)) \tag{7}$$

$$= \arg\min_{\boldsymbol{R}_{1:V}} \sum_{i=1}^{V} \log|\boldsymbol{R}_i| + \boldsymbol{e}_i^{\mathsf{T}} \boldsymbol{R}_i^{-1} \boldsymbol{e}_i. \tag{8}$$

$$\approx \arg\min_{G} \sum_{i=1}^{V} \log|g(\boldsymbol{\xi}_i)| + \boldsymbol{e}_i^{\mathsf{T}} g(\boldsymbol{\xi}_i)^{-1} \boldsymbol{e}_i \tag{9}$$

where G is the set of parameters of function g, i.e., the parameters of the neural network being optimized.

D. Decomposition for Positive Definiteness

The optimization in Eq. 9 is subject to all predictions $g(\boldsymbol{\xi}_i)$ being positive definite matrices. We would like to remove this constraint so that the function can be optimized using standard Stochastic Gradient Descent. To do this, we reformulate g to predict a decomposition of the covariance matrix $\boldsymbol{R}_i$, i.e., the free parameters $\boldsymbol{\alpha}_i \in \mathbb{R}^q$ where $q = \frac{n(n+1)}{2}$, instead of its vectorized form $\boldsymbol{r}_i \in \mathbb{R}^{n \times n}$. We then add a known function g_d that re-constructs the covariance matrix, i.e., splitting Eq. 3 into $\boldsymbol{R}_i \approx g_d(g_h(\boldsymbol{\xi}_i))$, where g_h is the new predictor function for the free parameters $\boldsymbol{\alpha}_i$:

$$\boldsymbol{\alpha}_i \approx g_h(\boldsymbol{\xi}_i) = \boldsymbol{W} \cdot f_k(\boldsymbol{\xi}_i) + \boldsymbol{b}. \tag{10}$$

We choose the LDL decomposition as in [4],

$$\boldsymbol{R}_i \approx g_d(\boldsymbol{\alpha}_i) = L(\boldsymbol{l}_i) D(\boldsymbol{d}_i) L(\boldsymbol{l}_i)^{\mathsf{T}} \tag{11}$$

where the free parameters $\boldsymbol{\alpha}_i = \left[\boldsymbol{l}_i, \boldsymbol{d}_i\right]^{\mathsf{T}}$ consist of a sub-vector $\boldsymbol{d}_i \in \mathbb{R}^n$ for reconstructing the diagonal matrix, and a sub-vector $\boldsymbol{l}_i \in \mathbb{R}^{(n^2-n)/2}$ for the lower unitriangular matrix. This decomposition exists and is unique for all positive definite matrices as long as the diagonal elements of $D(\boldsymbol{d}_i)$ are constrained to be positive. A simple way to enforce this constraint is to add an element-wise exponential function to the diagonal vector, i.e., update the diagonal matrix to be $D(\exp(\boldsymbol{d}_i))$. While any decomposition that does not impose difficult constraints on the free parameters $\boldsymbol{\alpha}_i$ would suffice, the LDL decomposition is particularly attractive due to its numeric stability in computing the log-determinant:

$$\begin{aligned} \log|\boldsymbol{R}_i| &= \log|L(\boldsymbol{l}_i) D(\exp(\boldsymbol{d}_i)) L(\boldsymbol{l}_i)^{\mathsf{T}}| \\ &= \log(|(D(\exp(\boldsymbol{d}_i))|) = \mathrm{sum}(\boldsymbol{d}_i), \end{aligned} \tag{12}$$

where $\mathrm{sum}(v)$ denotes the summation of the elements of the vector v. The final optimization problem is then

$$\begin{aligned} \arg\min_{G} \sum_{i=1}^{V} & \mathrm{sum}(\boldsymbol{d}_i) \\ & + \boldsymbol{e}_i^{\mathsf{T}} (L(\boldsymbol{l}_i) D(\exp(\boldsymbol{d}_i)) L(\boldsymbol{l}_i)^{\mathsf{T}})^{-1} \boldsymbol{e}_i, \end{aligned} \tag{13}$$

where $g_h(\boldsymbol{\xi}_i) \approx \boldsymbol{\alpha}_i = \left[\boldsymbol{l}_i, \boldsymbol{d}_i\right]^{\mathsf{T}}$. In the following section, we evaluate the accuracy of the covariance prediction function learned from solving the optimization problem.

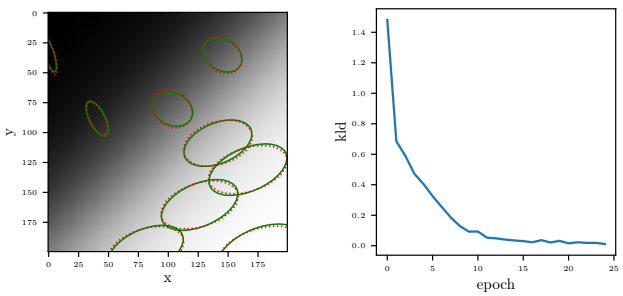

(a) Sample Covariances (b) KL divergence

Fig. 3: Predicted covariance ellipses (red) and ground-truth covariance ellipses (green) are shown for a few samples in the simulated map. It can be seen that the Kullback-Leibler divergence is quickly reduced in just 25 epochs.

IV. Simulation Results

A. Simulation Setup

To validate our approach, we first picked a virtual environment where we could simulate a sensor with known measurement covariances. Ground-truth covariances are normally difficult to obtain, but using a simulation environment circumvented this difficulty. We picked a simulated position sensor whose performance is correlated with the brightness of the location $\boldsymbol{x}_i \in \mathbb{R}^2$ within a 2D map $\boldsymbol{m} \in \mathbb{R}^{k \times k}$, i.e.,

$$\boldsymbol{R}_i = f(\boldsymbol{x}_i, \boldsymbol{m}). \tag{14}$$

We designed the ground-truth sensor noise model f, consisting of exponential and cosine functions, to introduce complex non-linear noise characteristics. We then randomly sampled 1000 locations $\boldsymbol{x}_i$ within a known map $\boldsymbol{m}$ and for each sample, computed the measurement covariance $\boldsymbol{R}_i$ from which to draw an error label $\boldsymbol{e}_i$, i.e.,

$$\boldsymbol{e}_i \sim \mathcal{N}(x_i, f(\boldsymbol{x}_i, \boldsymbol{m})). \tag{15}$$

We chose the local region of the map m around the robot position x_i to be the raw measurement $\boldsymbol{\xi}_i$, i.e.

$$\boldsymbol{\xi}_i = h(\boldsymbol{x}_i, \boldsymbol{m}), \tag{16}$$

and obtained the training set $\mathcal{D} = \{\boldsymbol{R}_i, \boldsymbol{e}_i, \boldsymbol{\xi}_i | \forall i \in [1, V]\}$.

B. Simulation Results

We optimized the objective function g in Eq. 13 using Stochastic Gradient Descent. Due to the simplicity of this problem, we were able to reduce the complexity of the function, removing convolution and reducing the network size. After optimizing for 25 epochs, we obtained predicted covariances $g(\boldsymbol{\xi}_i)$ for each raw measurement $\boldsymbol{\xi}_i$. With access to ground-truth covariance labels $\boldsymbol{R}_i$, we evaluated the Kullback-Leibler divergence (KLD) in Eq. 5 at each epoch.

As shown in Fig. 3, minimizing the negative log-likelihood quickly reduced KLD, an evidence of the alternative optimization in Eq. 6 reducing the direct distance metric. We also compared a few representative covariance predictions against the ground-truth for qualitative evaluation.

V. Experiment Results

A. Experiment Setup

We evaluated the performance of DICE on predicting the measurement covariances of the output of a 2D visual odometry (VO) algorithm based on DVO [8]. The algorithm densely aligns each RGB image to the previous image by projecting the image into the world using known depth information, then solving for the best back-projection into the previous image that minimizes the photometric error between the two. The difference between our 2D VO algorithm and standard DVO is that back-projection is limited to 2D motions, and no motion prior is used.

We chose the Microsoft Kinect as the raw measurement sensor to pair with the algorithm, creating a Kinect-DVO sensor that measures relative 2D motion. Based on the fact that the odometry is computed by minimizing a metric in the image-space (while the depth information is only used for projections) and the similarity of consecutive RGB images under moderate motion, we assumed that most predictive features of uncertainty are in the latest RGB image. We therefore chose only the latest RGB image as the input to our predictor function g, although the VO algorithm required both RGB images and a depth image to solve the alignment.

B. Training Data Collection

To generate training data, we collected RGB-D images in an environment equipped with a Vicon motion capture system. We obtained relative pose measurements using the Kinect-DVO sensor, and computed the error in the measurements as deviation from the Vicon measurements. We collected approximately 42,500 pairs of images and error labels as training data. In this experiment, we specifically explored two common failure modes of VO algorithms: low texture scenes and dynamic scenes. The environment was set up to include varying degrees of texture, and a person periodically walked in and out of the sensor frame during data collection. The objects in the environments were also moved around to prevent overfitting to the environment.

C. Network Structure and Training

While representing the covariance predictor as a CNN removes the need to carefully specify a parametric form of the covariance approximation function, high-level design choices (width, depth, etc) are required for the network.

We used an eight layer deep CNN and the input RGB images were down-sampled to 48x64 pixel greyscale images. Each of the two convolutional layers consisted of 32 kernels of size 5x5, followed by a 2x2 max pooling layer. Before the output, there was one fully connected layer of 256 units, and a dropout layer with a dropout rate of 50% to prevent overfitting. The network, visualized in Fig. 2, was trained using an Nvidia GeForce GTX 1080 for 6000 epochs, with a learning rate of 0.0001, a Nesterov momentum of 0.9, and a mini-batch size of 500. After experimenting with different nonlinear activation functions, we found that a leaky rectify activation [9] provided the most stable optimization.

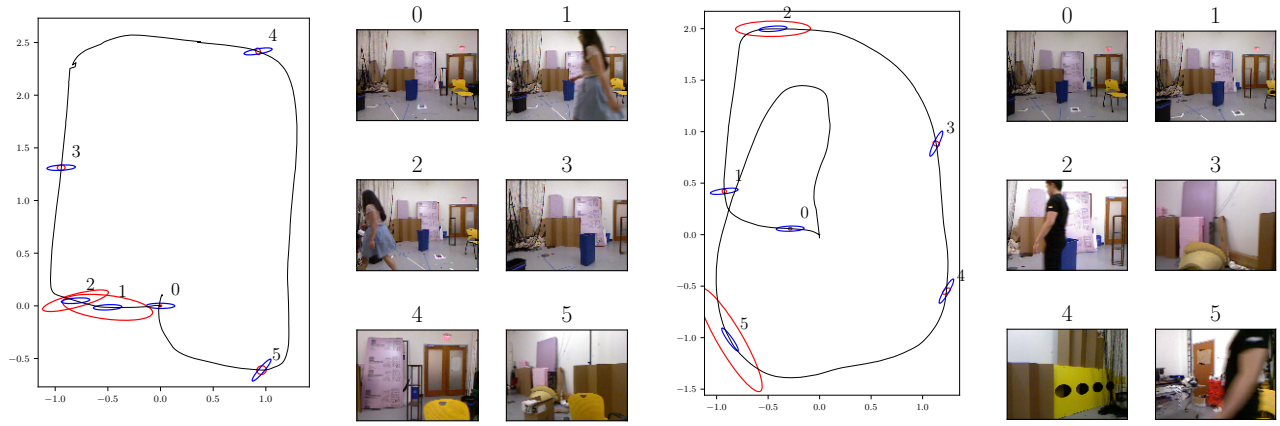

Fig. 4: Constant (blue) and DICE (red) measurement covariances are plotted for the *Dynamic* (left) and *Unseen-Dynamic* (right) datasets. The thumbnail images show the RGB frames at the correspondingly labeled points on the ground-truth trajectories (black). The constant covariance, which is empirically fit to the training data and non-spherical, underestimates the error in non-static scenes (i.e., 1 and 2 in *Dynamic*, 2 and 5 in *Unseen-Dynamic*) and overestimates in static scenes. DICE covariances vary largely both in magnitude and shape (larger and elongated in non-static scenes, while small and spherical in static scenes), more accurately representing the distribution of measurement error in different scenes. The major and minor axes of the covariance were enlarged by a factor of 20 for visualization purposes.

D. Test Sets

We chose four test sets to benchmark DICE:

- *Dynamic*: A person present in the training dataset walked across the camera frame once
- *White-wall*: The Kinect moved in a loop with two separate low texture scenes
- *Unseen-Dynamic*: A person *not* present in the training dataset walked across the camera frame twice
- *TUM*: This is the *freiburg3_walking_static* dataset (from the *TUM* [10] RGB-D SLAM benchmarks). The Kinect was static and two people walked in and out of frame

The first three, *Dynamic*, *White-wall* and *Unseen-Dynamic*, were drawn from the environments in the training data. For reporting the likelihood metric, we removed data points where Vicon measurements were measurably wrong (approximately 2% of the measurements).

E. Measurement Likelihood Performance

In real environments, we do not have access to the true distribution over measurement error to compare directly against the predicted distributions as done in Section IV. Instead, we could compare the likelihood of drawing true measurement errors from predicted distributions as in Eq. 6.

We benchmarked the covariance prediction performance of DICE against a constant covariance model, DVO's internal prediction based on the Cramer-Rao bound [11], and CELLO. To determine an appropriate constant covariance, we calculated a single covariance over all of the training data. The Cramer-Rao covariances were obtained by inverting the Fisher information matrices of the dense photometric alignment and multiplying by an empirically-determined factor to compensate for the bounds being lower-bounds and largely conservative. We used the empirical factor provided in the open-source implementation of DVO, noting that this parameter can also be tuned to perform arbitrarily well on any given dataset. The CELLO covariances were obtained using 10 image-space features proposed in [12] (e.g. dynamic range, pixel entropy, image gradients, etc) and the entire training dataset for DICE was used as potential neighbors in the kernel estimator. A few representative constant and DICE measurement covariances are shown in Fig. 4.

TABLE I: Mean log-likelihood results are shown for each prediction method and dataset pair. Values marked with † were generated after the prediction method was further trained with the augmented training dataset. On average, DICE predicted covariances better modeled the errors over all four test sets, and each DICE covariance prediction took approximately 0.01 seconds, in Python using a modern i7.

	Dynamic	*White-wall*	*Unseen-Dynamic*	*TUM*
Constant	9.20	8.84	9.27	8.62
Cramer-Rao	-26.72	-2.92	-29.06	4.95
CELLO	10.61	9.52	10.36	9.15†
DICE	**11.80**	**10.38**	**11.13**	**9.63**†

Table I summarizes the performance of the four methods on each test set described in Section V-D. We observed that on average, the covariances estimated by DICE better explained the observations than those of the other approaches. Fig. 6 illustrates the predictive performance of DICE on *Dynamic* test set; regions of the trajectory characterized by larger measurement error magnitudes were paired with larger covariance estimates by DICE. In comparison, the constant covariance method was unable to adapt, the Cramer-Rao approach was still a severe underestimate, and CELLO adapted but underestimated the magnitude of the covariance.

To test how well our method generalizes to new scenarios and environments, we considered the *Unseen-Dynamic*

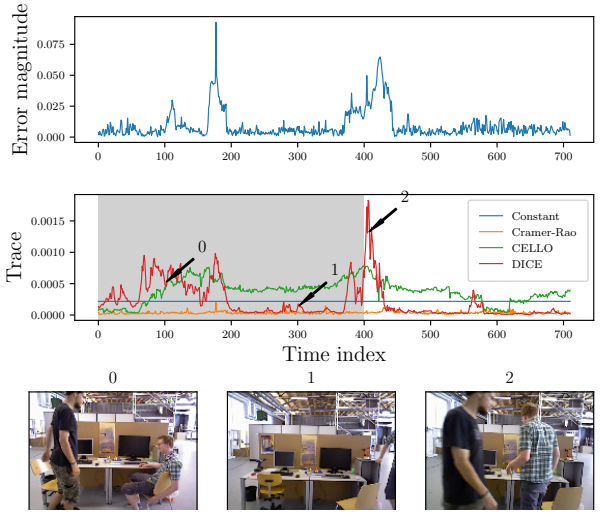

Fig. 5: The trace of the predicted measurement covariances of all four methods on the TUM dataset are shown, with representative images for small (1) and larger (0 and 2) magnitude trace predictions. The grey shaded region indicates the samples that were used to augment the existing training dataset, while the unshaded portions were reserved for testing. DICE outperforms the other three methods, predicting larger covariances in regions of higher error.

dataset. Although this dataset was set in the same environment as was used to train DICE, the person in this test set was not present in the training dataset. We observed that DICE predicted more likely measurement models, on average, than the other covariance prediction methods, indicating that the low-level representation was general to some degree.

To test the adaptability of our approach, we considered the *TUM* dataset, which has both an entirely new environment and new people. We augmented the original training dataset with the first 400 samples of the *TUM* dataset, and tuned the pre-trained network with the augmented dataset (for comparison purposes, we also augment the CELLO training dataset). The average log-likelihood results over the entire *TUM* dataset is reported in Table I. Fig. 5 illustrates that given examples of a new environment, DICE can be re-optimized to predict better measurement models than constant, Cramer-Rao, and CELLO models, better distinguishing the measurement error in static and dynamic scenes. This example further illustrates a strength of data-driven feature discovery, providing evidence that the predictions can be further improved in new environments by taking pre-trained models and resuming optimization on new data.

F. Trajectory Estimation Performance

We adapted the generic single-sensor trajectory optimization in Eq. 2 to test the utility of accurately predicting covariances of relative visual odometry measurements. Since our VO measurements fully observe the robot state relative to the previous state, the measurement model is simply $h(\boldsymbol{x}_i, \boldsymbol{x}_{i-1}) = \boldsymbol{x}_i - \boldsymbol{x}_{i-1}$. We removed the state transition model to best highlight the differences between covariance prediction methods, and added a ground-truth loop-closure

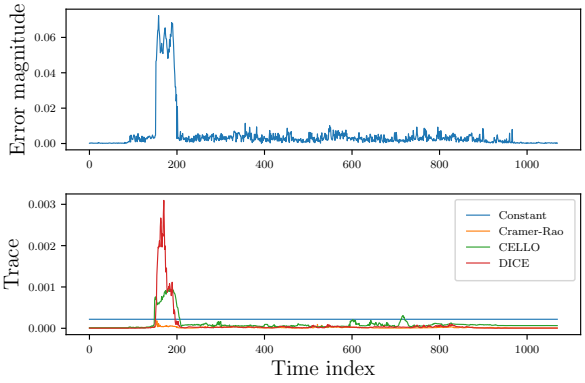

Fig. 6: Raw measurement errors in *Dynamic* test set are shown along with the trace of predicted covariances. The trace of DICE covariance is highly correlated with the error, demonstrating that DICE can accurately predict the uncertainty of the measurements.

TABLE II: Mean and standard error for the absolute positional error (meters) in the loop-closed trajectory are shown. DICE outperformed constant and Cramer-Rao approaches on every dataset, and for the *Dynamic* dataset where the error in the raw odometry was the greatest, the performance gain using DICE was also the greatest. In this dataset, the mean positional error in DICE was less than half of that of constant. Comparing DICE to CELLO, in datasets where CELLO's features were inadequate (dynamic scenes), DICE outperformed CELLO. For the dataset where the CELLO features were representative, DICE was tied with CELLO.

	Dynamic	*White-wall*	*Unseen-Dynamic*
Constant	0.57 ± 0.015	0.74 ± 0.013	0.70 ± 0.012
Cramer-Rao	0.59 ± 0.015	0.77 ± 0.011	0.67 ± 0.011
CELLO	0.37 ± 0.014	**0.50 ± 0.0093**	0.45 ± 0.010
DICE	**0.25 ± 0.011**	**0.50 ± 0.010**	**0.39 ± 0.010**

$s^* \in \mathbb{R}^p$ with a small covariance $\boldsymbol{S}$ between the first and the last states to observe the influence of covariances in loop-closing a warped trajectory. We solved the adapted problem

$$\underset{\boldsymbol{x}_{0:N}}{\arg\min} \sum_i^N \|\boldsymbol{x}_i - \boldsymbol{x}_{i-1} - \boldsymbol{z}_i\|^2_{\boldsymbol{R}_i} + \|\boldsymbol{x}_N - \boldsymbol{x}_0 - s^*\|^2_{\boldsymbol{S}} \quad (17)$$

with different sources of measurement covariances $\boldsymbol{R}_i$, and compared the absolute positional error in the loop-closed trajectory. Summarized in Table II, DICE significantly outperformed the other methods, reducing the average error by more than a factor of two in the Dynamic dataset. In this dataset, where a person walking across the camera corrupted the raw odometry, DICE assigned high covariances, distrusting the dynamic region and allowing the rest of the trajectory to be recovered more accurately (shown in Fig. 7). In comparison, CELLO distrusted the region noticeably less than DICE, while constant and Cramer-Rao methods equally trusted the dynamic region, resulting in the error from this region being distributed across the entire trajectory. Similar results were obtained for the *Unseen-Dynamic* test set, where a previously unobserved person came into the view.

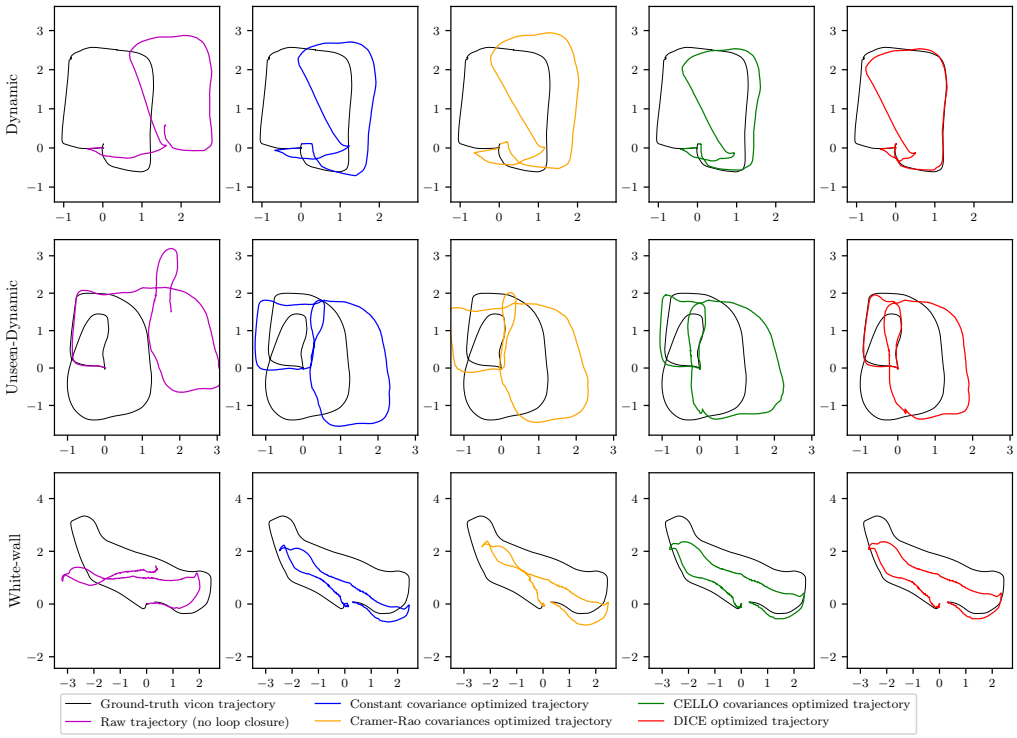

Fig. 7: Comparison of trajectory estimates in meters using constant, Cramer-Rao, CELLO, and DICE measurement covariances. Unlike constant and Cramer-Rao methods, DICE correctly associates the accumulated error in the raw odometry (shown in magenta) to regions of high measurement error (textureless/dynamic), accurately estimating other parts of the trajectory when optimized with a loop-closure. On the other hand, loop-closing with constant measurement covariances distributes the total accumulated error equally across the entire trajectory, deforming even regions with low measurement error. For example, there is a region of high measurement error in the beginning of the *Dynamic* dataset due to a person walking across the camera frame. DICE predicts a larger noise in this region (see Fig.4), and is able to better estimate the remaining trajectory. Deformation in regions where DVO exhibits large measurement errors could also be improved if there was a second source of odometry that is characterized by lower measurement error in those regions (e.g., an IMU).

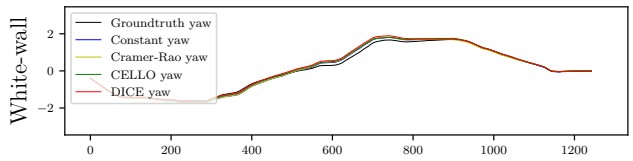

Fig. 8: Comparison of orientation estimates (radians) using constant, Cramer-Rao, CELLO, and DICE covariances. The orientation tracking of all methods is comparable.

Additionally, in the *White-wall* dataset, DICE performed significantly better than constant and Cramer-Rao methods, but was on par with CELLO. We observed that for failure modes that are well explained by the hand-coded features of CELLO (i.e., white walls form a tight cluster in the feature space defined using image-space statistics), CELLO could perform as well as DICE. However, for failure modes that are difficult to explain with the expert-specified features, DICE outperformed CELLO, demonstrating the utility of learning the feature space directly from the data.

In terms of the average rotational error, there was no significant difference between the covariance prediction methods. The different methods were relatively accurate in estimating the orientation, and the empirically-fit constant covariances often performed the best. In the *White-wall* dataset shown in Fig. 8, the constant covariance method outperformed DICE by 3.3 degrees, and this was the greatest difference across all datasets. In conclusion, we observed that in cases where the estimates were noisy, DICE out-performed other methods by a significant margin, while in cases where the raw estimates were accurate, DICE performed similarly.

VI. Related Works

Early approaches to covariance estimation were largely reactive methods. These approaches include adaptive Kalman filtering [13] and multiple model adaptive estimation methods [14]. The reactive nature of these approaches can cause latency in the evolution of the noise model and be sensitive to the window of measurements used to calculate statistics.

Another approach to covariance estimation is to specify noise models for specific sensor-algorithm pairs. For example, [15] and [16] developed covariance functions for laser-based sensors (e.g. LIDARs) coupled with iterative-closest-point (ICP) algorithms. Given that these approaches are designed for specific sensors, it can be difficult to generalize the results to a more diverse set of sensors and algorithms.

There is a significant body of literature regarding non-parametric approaches to predictive covariance estimation. For example, Ko et. al. [17] described how to use Gaussian Processes to estimate heteroscedastic Gaussian noise models, and Tallavajhula et. al. [18] proposed generic non-parametric noise models. However, these types of approaches also suffer from scaling problems without a lower-dimensional feature space. We note that feature specification is itself a topic of research, as in [19], which experimentally designs expertly hand-coded features for use in covariance estimation.

The neural network community has also previously estimated arbitrary probability distributions for joint [20] and conditional distributions [21], but proper backpropagation proved to be computationally expensive. Williams described how neural networks could be used to model conditional multivariate densities [22], proposing special "dispersion" nodes to learn the parameters of a Cholesky decomposition. They demonstrate the approach on one and two dimensional examples, and extend to time series financial data.

Recent work [23], [24] using neural networks to estimate uncertainties adopt similar log-likelihood models to ours. [23] assumes a diagonal covariance matrix and estimates the mean as well as the covariance of a specific end-to-end learned VO sensor. [24] combines heterodescedatic aleatoric noise, which we model, with epistemic noise in a single model, but is orders of magnitude slower due to the expensive Monte Carlo sampling required for the epistemic noise.

VII. Conclusion

We have presented DICE – a novel method for predicting measurement noise of complex sensors without using extensive domain knowledge. We demonstrated that DICE can accurately predict the measurement covariance of a simulated light sensor, and a visual odometry sensor. We have shown that predicting accurate measurement covariances can help improve trajectory estimates, and achieve accuracy significantly better than conventional methods for difficult scenes.

Acknowledgment

This work was supported by NASA under Award No. NNX15AQ50A and DARPA under Fast Lightweight Autonomy (FLA) program, Contract No. HR0011-15-C-0110.

References

[1] J. Engel, T. Schöps, and D. Cremers, "LSD-SLAM: Large-scale direct monocular SLAM," in *ECCV 2014*.

[2] K. Ok, W. N. Greene, and N. Roy, "Simultaneous tracking and rendering: Real-time monocular localization for MAVs," in *Proc. ICRA 2016*.

[3] W. Vega-Brown, A. Bachrach, A. Bry, J. Kelly, and N. Roy, "CELLO: A fast algorithm for covariance estimation," in *Proc. ICRA 2013*.

[4] H. Hu and G. Kantor, "Parametric covariance prediction for heteroscedastic noise," in *Proc. IROS 2015*.

[5] F. Dellaert and M. Kaess, "Square root sam: Simultaneous localization and mapping via square root information smoothing," *IJRR*, vol. 25, no. 12,

[6] Q. V. Le, "Building high-level features using large scale unsupervised learning," in *Proc. ICASSP 2013*.

[7] K. Simonyan and A. Zisserman, "Very deep convolutional networks for large-scale image recognition," *arXiv:1409.1556*, 2014.

[8] C. Kerl, J. Sturm, and D. Cremers, "Robust odometry estimation for RGB-D cameras," in *Proc. ICRA 2013*.

[9] A. L. Maas, A. Y. Hannun, and A. Y. Ng, "Rectifier nonlinearities improve neural network acoustic models," in *Proc. ICML*, vol. 30, 2013.

[10] J. Sturm, N. Engelhard, F. Endres, W. Burgard, and D. Cremers, "A benchmark for the evaluation of RGB-D SLAM systems," in *Proc. IROS*, 2012.

[11] C. R. Rao, "Information and the accuracy attainable in the estimation of statistical parameters," *Bull. Calcutta Math. Soc.*, vol. 37, pp. 81–89, 1945.

[12] W. Vega-Brown, "Predictive parameter estimation for bayesian filtering," Master's thesis, Massachusetts Institute of Technology, 2013.

[13] R. Mehra, "On the identification of variances and adaptive Kalman filtering," *IEEE Transactions on Automatic Control*, vol. 15, no. 2, pp. 175–184, 1970.

[14] D Magill, "Optimal adaptive estimation of sampled stochastic processes," *IEEE Transactions on Automatic Control*, vol. 10, no. 4, pp. 434–439, 1965.

[15] A. Censi, "An accurate closed-form estimate of ICP's covariance," in *Proc. ICRA 2007*.

[16] M. Barczyk and S. Bonnabel, "Towards realistic covariance estimation of ICP-based Kinect V1 scan matching: The 1D case," in *Proc. ACC 2017*.

[17] J. Ko and D. Fox, "GP-BayesFilters: Bayesian filtering using Gaussian process prediction and observation models," *Autonomous Robots*, vol. 27, no. 1,

[18] A. Tallavajhula, B. Póczos, and A. Kelly, "Nonparametric distribution regression applied to sensor modeling," in *Proc. IROS 2016*.

[19] V. Peretroukhin, L. Clement, M. Giamou, and J. Kelly, "PROBE: Predictive robust estimation for visual-inertial navigation," in *Proc. IROS 2015*.

[20] D. S. Modha and Y. Fainman, "A learning law for density estimation," *IEEE Transactions on Neural Networks*, vol. 5, no. 3, pp. 519–523, 1994.

[21] A. Sarajedini, R. Hecht-Nielsen, and P. M. Chau, "Conditional probability density function estimation with sigmoidal neural networks," *IEEE Transactions on neural networks*, vol. 10, no. 2, pp. 231–238, 1999.

[22] P. M. Williams, "Using neural networks to model conditional multivariate densities," *Neural Computation*, vol. 8, no. 4, pp. 843–854, 1996.

[23] S. Wang, R. Clark, H. Wen, and N. Trigoni, "End-to-end, sequence-to-sequence probabilistic visual odometry through deep neural networks," *IJRR*, p. 0 278 364 917 734 298, 2017.

[24] A. Kendall and Y. Gal, "What uncertainties do we need in bayesian deep learning for computer vision?" In *Proc. NIPS*, 2017.